



Cite this: *Sustainable Energy Fuels*, 2021, 5, 144

Benzothiadiazole-based photosensitizers for efficient and stable dye-sensitized solar cells and 8.7% efficiency semi-transparent mini-modules†

Maxime Godfroy, ^a Johan Liotier, ^a Valid M. Mwalukuku, ^a Damien Joly, ^a Quentin Huault, ^a Lydia Cabau, ^a Cyril Aumaitre, ^a Yann Kervella, ^a Stéphanie Narbey, ^b Frédéric Oswald, ^b Emilio Palomares, ^{cd} Carlos A. González Flores, ^e Gerko Oskam ^{ef} and Renaud Demadrille ^{aa}

We report on the synthesis and structure–properties relationships of five benzothiadiazole-based organic dyes designed for use in Dye-Sensitized Solar Cells (DSSCs). These compounds exhibit hues ranging from pink to violet-blue and demonstrate good Power Conversion Efficiencies (PCEs) ranging from 7.0% to 9.8% when employed as photosensitizers with TiO_2 mesoporous electrodes. The combination of two of these dyes following a co-sensitization approach led to a PCE of up to 10.9% with an iodine-based liquid electrolyte. We demonstrate, using charge extraction and transient photo-voltage experiments, that the improvement of the performances with the cocktail of dyes is related to better light absorption and passivation of the TiO_2 surface. When the volatile electrolyte is swapped for an ionic-liquid, PCEs over 7.5% are reached and the best solar cells retain 80% of their initial performance after 7000 h of light exposure, according to the accelerated aging test ISOS-L2 (65 °C, AM1.5G, under continuous irradiation at 1000 W m⁻²). Finally, we report excellent performance in five-cell mini-modules with 14 cm² active area demonstrating a PCE of 8.7%. This corresponds to a power output of *circa* 123 mW, ranking among the highest performances for such semi-transparent photovoltaic devices.

Received 8th September 2020
Accepted 22nd October 2020

DOI: 10.1039/d0se01345e
rsc.li/sustainable-energy

1. Introduction

During the past two decades, tremendous efforts have been focused on the development of photovoltaic (PV) technologies capable of palliating some of the drawbacks of conventional silicon-based solar panels such as heaviness, opaqueness and large energy consumption during manufacturing.^{1,2} Technologies integrating organic and hybrid materials such as Dye-Sensitized Solar Cells (DSSCs),^{3,4} Bulk-Hetero-Junction solar cells (BHJ),^{5–7} or Perovskite Solar Cells (PSC)^{8,9} have progressed significantly. Nowadays they appear to be adapted to solve some of these drawbacks.¹⁰ In terms of power conversion efficiencies (PCEs), the best DSSCs performances lie in the range of 10 to

14.2%,^{11–15} which is lower compared to BHJ and PSC, but interestingly they already demonstrated superior long-term stability. Indeed, when non-volatile electrolytes are employed,^{16–18} their performance can be conserved under harsh testing conditions,¹⁶ and a stability corresponding to approximately 10 years of use in real conditions has been demonstrated. Besides, this technology enables the fabrication of semi-transparent solar panels that can be colourful and prepared with non-toxic constituents.¹⁹ All these criteria make DSSCs very appealing for Building-Integrated Photovoltaics (BIPV)^{18,20,21} or Automobile Integrated Photovoltaics (AIPV).²² The performance of a DSSC mainly depends on the molecular structure of the dye used to photosensitize the mesoporous electrode. Historically, Ru(II)-polypyridyl complexes were the first efficient dyes used as photosensitizers in DSSCs (N-719 or N-749)²³ but they possess low absorption coefficients in the visible range,²⁴ and contain ruthenium which is a rare and high-cost element. Besides, their plausible toxicity restrains their development at the industrial level. Consequently, metal-free organic dyes based on the donor-(π -spacer)-acceptor structure have been extensively developed, studied and screened as photosensitizers in DSSCs.^{25,26}

To improve the photocurrent generation and hence photovoltaic performances of DSSCs, the development of new dyes better matching the solar emission spectrum appeared to be an

^aUniv. Grenoble Alpes, CNRS, CEA, INAC, SyMMES, 17 rue des martyrs, 38000 Grenoble, France. E-mail: renaud.demadrille@cea.fr

^bSolaronix SA, Rue de l'Ouriette 129, 1170 Aubonne, Switzerland

^cInstitute of Chemical Research of Catalonia (ICIQ), Avenguda Països Catalans, 16, Tarragona 43007, Spain

^dICREA, Passeig Lluís Companys, 23, Barcelona E-08010, Spain

^eDepartment of Applied Physics, CINVESTAV-IPN, Mérida, Yucatán, 97310, México

^fDepartamento de Sistemas Físicos, Químicos y Naturales, Universidad Pablo de Olavide, Carretera de Utrera km 1, Sevilla 41013, Spain

† Electronic supplementary information (ESI) available: Synthesis, spectroscopy, modelling, solar cells. CCDC 2030933 and 2030934. For ESI and crystallographic data in CIF or other electronic format see DOI: 10.1039/d0se01345e



efficient strategy. A decade of development led to a plethora of new organic dyes, allowing identification of very efficient electron-rich units (such as triarylamine derivatives) and anchoring electron-withdrawing units (such as cyanoacrylic acid or carboxylic acid) for their preparation.²² Many chromophores have been also investigated as π -conjugated spacers (BODIPY,²⁶ isoindigo,²⁷ porphyrins^{12,28,29}) to tune their optoelectronic properties. A few years ago, we reported a benzothiadiazole-containing dye, namely **RK1**,¹⁶ showing a rather simple chemical structure and demonstrating a power conversion efficiency of up to 10.2% with an outstanding stability of more than 9000 hours when subjected to a harsh accelerated ageing test (ISOS-L2). This orange-reddish dye was the first purely organic photosensitizer to be implemented in a large semi-transparent module (active area of 1400 cm²) suitable for BIPV.²¹ Inspired by the design of this dye, we reported in 2018 another benzothiadiazole-based molecule namely **YKP-88**, where the TPA unit is bridged to the thiophene ring to form an indeno[1,2-*b*]thiophene unit. This dye showed an efficiency of over 9% in DSSCs fabricated with classical architectures, and up to 10.3% with inverse opals-based electrodes.³⁰ Consequently, in this work, we investigate further the performance of **YKP-88** and report the synthesis of four new analogue compounds whose chemical structures are tuned with the goal to shift its Internal Charge Transfer (ICT) absorption band towards lower energy wavelengths while keeping control of the energy levels of the frontier orbitals. Our objective was to prove efficient and stable dyes following this molecular concept while obtaining various colours. Their optoelectronic properties have been studied by UV-Vis spectroscopy, cyclic voltammetry (CV) and then compared to DFT calculations. We implemented these dyes in DSSCs using opaque TiO₂ electrodes and various electrolytes and we report their photovoltaic performances. The combination of **YKP-88** with one of the new dyes, following a co-sensitization approach, led to a PCE of up to 10.9% using an iodine-based electrolyte. The reasons behind the improvement of the performances were unravelled thanks to Charge Extraction (CE) and Transient Photo-Voltage (TPV) measurements. We also report, using ionic liquid-based electrolyte, stable solar cells that retain 80% of their initial efficiency for over 7000 hours when subjected to a standard ISOS-L2 accelerating ageing test. Finally, we show that semi-transparent mini-modules with an active surface of 14.08 cm² (total surface of 23 cm²) can be fabricated with **YKP-88**. This mini-module reached a PCE of 8.7% with a power output of *circa* 123 mW.

2. Results and discussion

2.1 Design and synthesis

Owing to the good efficiency and stability of DSSCs sensitized with **RK1** or **YKP-88** and the relatively ease of synthesis of these dyes, we developed in this study new molecules presenting a rather close chemical design. Fig. 1 presents the chemical structures of **RK1**, **YKP-88** and the 4 new dyes synthesized in this work. With the goal to shift the absorption of the new dyes towards longer wavelengths in the visible range, we tuned the push-pull effect within the molecules by increasing the

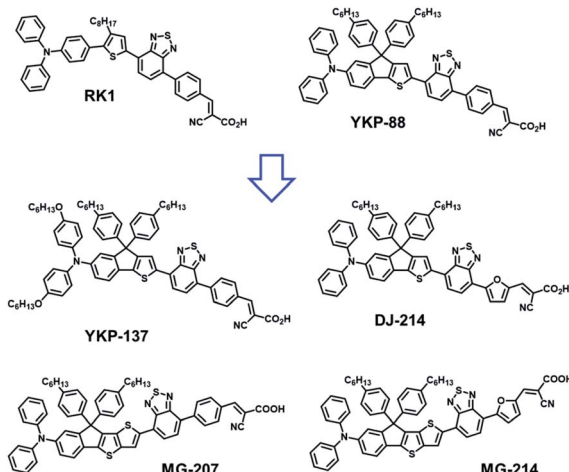


Fig. 1 Chemical structure of the previously reported dye **RK1**, **YKP-88** and structures of the four new dyes synthesized in this work.

electron-donating strength of the triarylamine (TPA) unit or by improving the planarity of the molecules (see X-ray structures in ESI†) and/or the π -conjugation with the electron-accepting unit. First, the TPA unit was substituted with two alkoxy groups to give **YKP-137**, second the replacement of the thiophene flanking the indene ring by a thiophene[3,2-*b*]thiophene unit was performed to give **MG-207**. Then we swapped the benzene spacer between the benzothiadiazole and the anchoring function for a furan unit.

This replacement led to a better planarization and conjugation of the electron-accepting units.³¹ Therefore, we obtained **DJ-214** and **MG-214** that are analogues of **YKP-88** and **MG-207**, respectively. The synthesis routes towards these 4 new dyes are presented in Fig. 2. The synthesis involves, as a precursor, ethyl-5-bromo-2-iodobenzoate that can be coupled with a thiophene unit through a Suzuki coupling or a thiophene[3,2-*b*]thiophene unit through a Negishi coupling to give compounds **1** and **8**, respectively. From **1**, 6-bromo-4,4-bis(4-hexylphenyl)-4*H*-indeno[1,2-*b*]thiophene, **2** can be obtained *via* Grignard reaction and cyclization under acidic conditions.³⁰ Applying the same approach starting from **8** afforded compound **9**. The triarylamine units **3**, **4** and **10** were obtained *via* Buchwald–Hartwig cross-coupling reaction using unsubstituted or alkoxy-substituted diphenylamine. Regioselective lithiation of **3** and **4** followed by a nucleophilic substitution with chlorotrimethylstannane afforded two stannylated intermediates, which were not isolated due to poor chemical stability. The intermediate corresponding to **4** was subsequently used in a Stille cross-coupling reaction with 4-(7-bromobenzo[*c*][1,2,5]thiadiazol-4-yl)benzaldehyde³² to give compound **7**. The stannylated derivative of **3** was reacted with 5-(7-bromobenzo[*c*][1,2,5]thiadiazol-4-yl)furan-2-carbaldehyde, **5**, to afford compound **6**. On the other hand, compound **10** was lithiated selectively to allow the formation of an organo-zinc intermediate by nucleophilic substitution with zinc chloride. This organo-zinc intermediate was then involved in a Negishi coupling with 4-(7-bromobenzo[*c*][1,2,5]thiadiazol-4-yl)



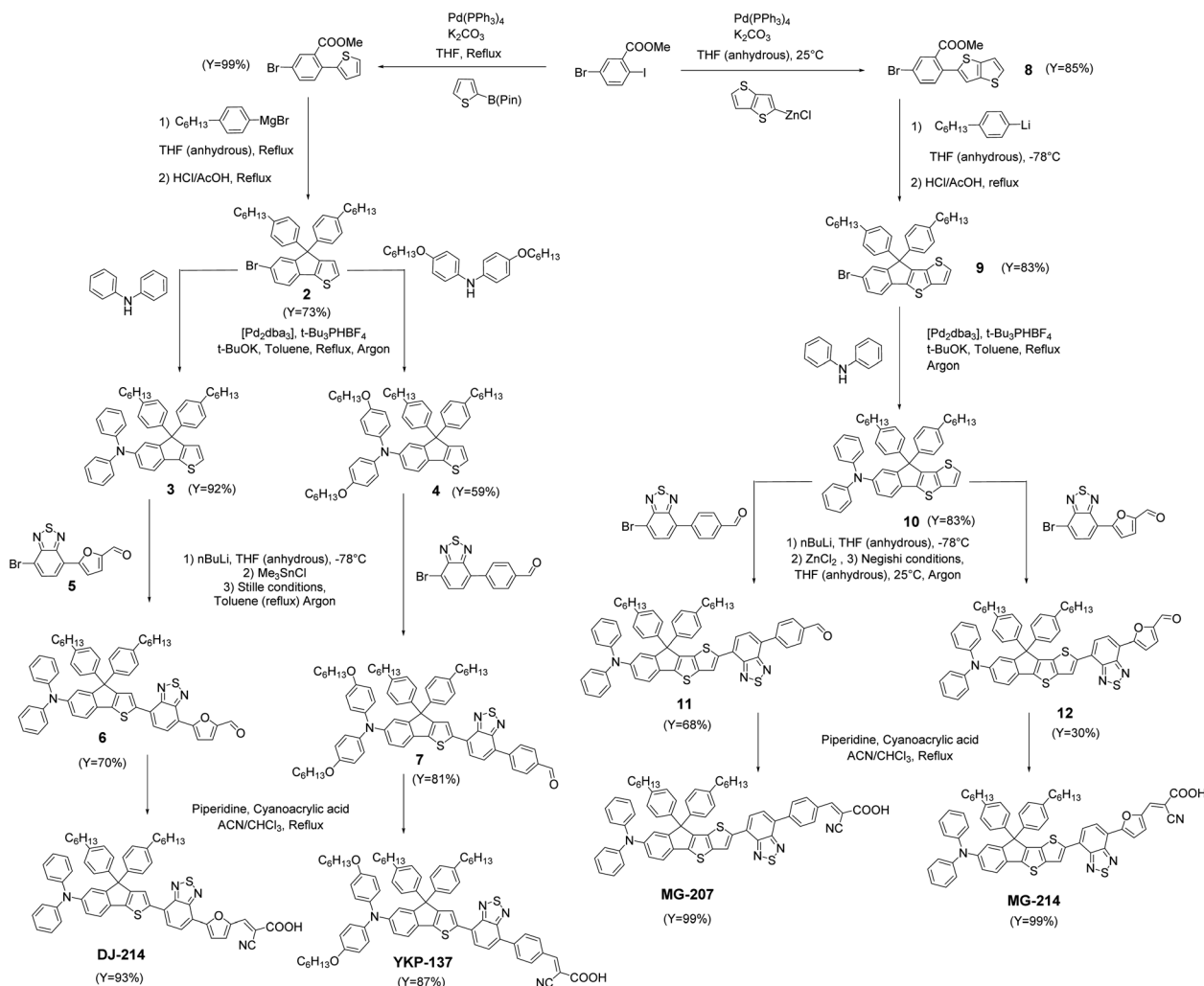


Fig. 2 Synthetic routes and intermediates towards YKP-137, DJ-214, MG-207 and MG-214 dyes.

benzaldehyde to give compound **11** and with 5-(7-bromobenzo[c][1,2,5]thiadiazol-4-yl)furan-2-carbaldehyde, **5**, to give compound **12**. The targeted materials **YKP-137**, **DJ-214**, **MG-207** and **MG-214** were obtained *via* Knoevenagel condensation with cyanoacetic acid in the presence of piperidine (synthetic procedures, $^1\text{H-NMR}$, $^{13}\text{C-NMR}$, HRMS and elemental analysis are given in ESI \dagger).

2.2 Optoelectronic properties

The optical properties of the compounds **YKP-137**, **DJ-214**, **MG-207** and **MG-214** were investigated and compared to those of **YKP-88**. When the dyes are evaluated in diluted solution (10^{-5} M in dichloromethane) (see Fig. 3a), they all display intense absorption in the visible range with molar extinction coefficients, at λ_{max} , comprised between 2.7×10^4 and $4.33 \times 10^4 \text{ L mol}^{-1} \text{ cm}^{-1}$. The absorption band located at lower energy is attributed to the Internal Charge Transfer (ICT) transition, whereas the other transition (around 400 nm) is attributed to the $\pi-\pi^*$ transitions of the different aromatic units. As expected, increasing the electronic density difference between the

electron donating and the withdrawing part implies a bathochromic shift of the Internal Charge Transfer (ICT) band. Thus, the alkoxy substituents introduced on the TPA unit of **YKP-137** induce a red shift of the ICT band by 28 nm compared to **YKP-88**. On the other hand, the replacement of the thiophene by a thiophenothiophene unit in **MG-207** has a minor effect on the λ_{max} with a small bathochromic shift (+3 nm). However, the shift is more pronounced for the UV absorption band (+12 nm). If the absorption spectra of **YKP-88** and **MG-207** are compared to the ones of **DJ-214** and **MG-214** respectively, we can probe the effect of swapping the benzene spacer for a furan. A strong bathochromic shift of λ_{max} is now observed (+52 nm) accompanied by a significant hyperchromic shift. This observation can be explained by the smaller resonance energy of furan compared to benzene (16 kcal mol^{-1} vs. 36 kcal mol^{-1}) leading to more effective conjugation. 33 Besides, our results confirm (see Fig. S1 in ESI \dagger) that using a furan spacer, a higher degree of planarity along the molecule is achieved. 34 The dihedral angle of 20° between the benzothiadiazole unit and the phenyl in **YKP-88** is reduced to 0° between the benzothiadiazole unit and the furan in **DJ-214**, leading to a perfect co-planarity and a better



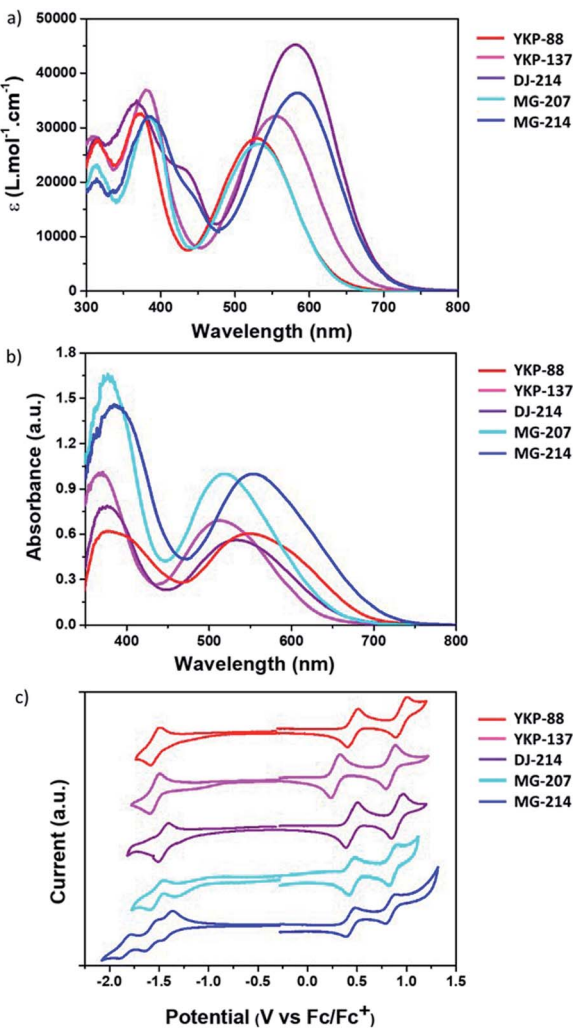


Fig. 3 (a) Absorption spectra registered (a) in Dichloromethane solution, (10^{-5} M, 25 °C), (b) on 2 μm -thick mesoporous TiO_2 electrodes, for compounds YKP-88 (red line), YKP-137 (magenta line), DJ-214 (violet line) MG-207 (cyan line) and MG-214 (blue line) (c) cyclic voltammetry traces in solution for each compound (deoxygenated dichloromethane, 10^{-3} M, 25 °C, voltage scan 200 mV s $^{-1}$).

conjugation with the anchoring function. The introduction of the furan unit also induces the emergence of an absorption shoulder between 400–450 nm.³¹

Table 1 Selected optical and electronic properties of compounds YKP-88, YKP-137, DJ-214, MG-207, MG-214

Dyes	$\lambda_{\text{max,vis}}^a$ [nm]	ϵ [$\text{M}^{-1}\text{cm}^{-1}$]	$E_{\text{opt}}^{a,b}$ [eV]	$\lambda_{\text{max, TiO}_2}^c$ [nm]	HOMO ^d [eV]	LUMO ^d [eV]	E_{elec}^e [eV]
YKP-88	529	28 100	1.99	513	-5.26	-3.26	2.00
DJ-214	582	45 300	1.79	550	-5.25	-3.35	1.90
YKP-137	557	32 200	1.87	533	-5.08	-3.26	1.82
MG-207	532	27 000	1.99	519	-5.25	-3.30	1.95
MG-214	584	36 400	1.81	554	-5.24	-3.40	1.84

^a In solution (DCM, 10^{-5} M) or adsorbed on anatase- TiO_2 (2 μm). ^b Calculated from $1241/\lambda_{\text{onset}}$. ^c TiO_2 electrode (thickness 2 μm), dyeing solution CHCl_3/t -butanol, 0.2 mM dye. ^d All potentials were obtained by cyclic voltammetry investigations in 0.2 M Bu_4NPF_6 in CH_2Cl_2 . The platinum electrode diameter was 1 mm and the sweep rate 200 mV s $^{-1}$. Potentials measured vs. Fc/Fc^+ and the values are calculated using half-wave potentials ($E_{1/2}$) and -4.8 eV as a Fc/Fc^+ standard *versus* vacuum level. ^e Calculated from $E_{\text{elec}} = E_{\text{HOMO}} - E_{\text{LUMO}}$.

The new compounds exhibit bright colours ranging from pink to violet-blue in solution. In order to gain more insights into the behaviour of these dyes once adsorbed on mesoporous TiO_2 , their absorption spectra were measured after grafting on a 2 μm -thick TiO_2 mesoporous layer from a 2 mM solution in a 1/1 mixture of ACN and *t*BuOH (see Table 1). Once the dyes are attached onto TiO_2 , their absorption spectra are broadened and the ICT band is blue-shifted by 16 nm, 24 nm and 13 nm for YKP-88, YKP-137 and MG-207 respectively, whereas the shift is more important *i.e.* 32 nm and 30 nm for DJ-214 and MG-214 (see Fig. 3b). A small blue shift is often observed when organic photosensitizers are grafted on the TiO_2 surface, which can be ascribed partly to the deprotonation of the carboxylic acid function.³⁵ However, larger shifts and broadening of the spectrum can be associated to the formation of aggregates,^{36,37} which is consistent with the more planar nature of the furan-containing molecules.

To get more insights into the optoelectronic properties of the compounds, cyclic voltammetry experiments were carried out with the objective to determine highest occupied molecular orbital (HOMO) and lowest unoccupied molecular orbital (LUMO) energy level positions (see Fig. 3c). We estimated the energy levels from their oxidation and reduction potential after calibration with ferrocene (Fc/Fc^+). Similar to YKP-88, the dyes DJ-214, MG-207 and MG-214 exhibit two reversible oxidation waves located at around +0.45 V and +0.95 V. YKP-137 is easier to oxidize because of the presence of alkoxy substituents on the TPA unit and hence its oxidation waves are found around +0.28 V and +0.86 V (see Fig. 3c). It clearly appears that the TPA unit dictates the HOMO energy level position. For all the dyes, the HOMO is around -5.25 eV except for YKP-137 whose HOMO is at -5.08 eV. Regarding the reduction process, it appears that the reduction potentials are similar for YKP-88 and YKP-137 (around -1.55 V), *i.e.* the dyes showing the same π -conjugated backbone. The reduction waves are shifted towards more positive potentials for the dyes in which the π -conjugated backbone is modified *i.e.* MG-207, DJ-214 and MG-214 (-1.50 V, -1.45 V and -1.40 V respectively). The LUMO energy levels are lying between -3.26 eV and -3.30 eV for the 3 dyes with a benzene spacer, and as expected, they are shifted towards more negative values for the dyes with a furan spacer.³⁸ This is another manifestation of the higher degree of conjugation between the electron-accepting unit and the benzothiadiazole unit. The



HOMO and LUMO energy levels of the dyes are positioned correctly with respect to the conducting band (CB) energy level of the TiO_2 and the redox potential of the iodine/iodide electrolyte, to warrant an efficient electron photo-injection from the dye to the TiO_2 and a good regeneration of the oxidised dye by the redox mediator. Consequently, we have fabricated DSSCs using this device configuration.

2.3 Dye-Sensitized Solar Cells

2.3.1 Evaluation of the performances of the photosensitizers. In order to characterize the photovoltaic behaviour of the dyes, DSSC were fabricated (see procedure in ESI[†]), and their current–voltage characteristics were recorded using a 0.36 cm^2 mask under AM1.5G irradiation at 1000 W m^{-2} .

Two types of electrolytes containing I^-/I_3^- redox couple were employed, first, a liquid electrolyte (Iodolyte HI-30) to achieve high performances and second, an ionic liquid-based electrolyte (Mosalyte TDE-250) to obtain more robust solar cells. The electrode thicknesses were optimized for each device configuration. Thick electrodes with 10 to 14 μm -thick mesoporous TiO_2 films coated with a 3 to 4 μm -thick reflecting layer were prepared and used with the liquid electrolyte. Thinner mesoporous layers (8 μm -thick coated with a 3 μm -thick reflecting layer) were employed to facilitate the complete filling of the

pores with Mosalyte TDE-250 because it shows higher viscosity. Some of the devices were fabricated in a double-blind process at Solaronix and at CEA, and the performances are as reported in Table 2 to prove the reliability and reproducibility of the results. The performances were compared to those obtained using **RK1** as a reference dye.^{11,16}

As can be noticed from this table, when used with a liquid electrolyte based on a low viscosity solvent, the five new dyes exhibit relatively good efficiencies, ranging from 7.01% up to 9.78% for the best cells. Notably, J_{sc} values over 14.5 mA cm^{-2} are measured with all the dyes. The performances of the DSSCs sensitized with the compounds embedding a phenyl spacer are higher than the ones arising from the dyes with a furan. One noticeable difference concerns the lower V_{oc} values obtained when a furan spacer is used. V_{oc} mean-values are up to 708 mV, 726 mV and 704 mV for compounds **YKP-88**, **YKP-137** and **MG-207** respectively, whereas with **DJ-214** and **MG-214** they are lowered by *circa* 40 to 60 mV. The highest V_{oc} is obtained with **YKP-137**, because of the presence of alkoxy-chains on the TPA that is known to lower the recombination rate.^{39–41} The loss of V_{oc} when a furan is inserted close to the anchoring group was expected since several teams have reported this phenomenon before. In previous studies, the V_{oc} drop was attributed to an

Table 2 Photovoltaic parameters of compounds **YKP-88**, **YKP-137**, **DJ-214**, **MG-207** and **MG-214**, under irradiation AM1.5G at 1000 W m^{-2} ; Electrodes: TiO_2 mesoporous anatase + scattering layer

Dyes	Electrolyte	TiO_2 electrode (μm)	J_{sc} (mA cm^{-2})	V_{oc} (mV)	FF (%)	PCE (%)
YKP-88	Iodolyte	$14 + 3^a$	17.89	735	72	9.52
YKP-88	Iodolyte	$14 + 3^b$	18.96	706	71	9.54
YKP-88	Iodolyte	$14 + 3^b$	18.66 ± 0.31	708 ± 3	71 ± 1	9.34 ± 0.12
YKP-88	Mosalyte TDE-250	$8 + 3^b$	17.39	642	66	7.36
YKP-88	Mosalyte TDE-250	$8 + 3^b$	16.81 ± 0.46	645 ± 3	67 ± 1	7.27 ± 0.04
DJ-214	Iodolyte	$14 + 3^a$	17.03	648	69	7.57
DJ-214	Iodolyte	$10 + 4^b$	17.08	670	71	8.09
DJ-214	Iodolyte	$10 + 4^b$	17.14 ± 0.06	666 ± 4	71 ± 0	8.08 ± 0.02
DJ-214	Mosalyte TDE-250	$8 + 3^b$	17.21	616	69	7.34
DJ-214	Mosalyte TDE-250	$8 + 3^b$	16.80 ± 0.41	613 ± 4	67 ± 3	6.87 ± 0.47
YKP-137	Iodolyte	$14 + 3^a$	19.50	723	68	9.55
YKP-137	Iodolyte	$10 + 4^b$	18.56	729	70	9.38
YKP-137	Iodolyte	$10 + 4^b$	18.52 ± 0.05	726 ± 4	69 ± 1	9.21 ± 0.18
YKP-137	Mosalyte TDE-250	$8 + 3^b$	15.70	659	63	6.59
YKP-137	Mosalyte TDE-250	$8 + 3^b$	15.61 ± 0.10	660 ± 0	61 ± 2	6.44 ± 0.16
MG-207	Iodolyte	$14 + 3^a$	22.14	672	66	9.78
MG-207	Iodolyte	$12 + 3^{b,c}$	18.42	703	73	9.41
MG-207	Iodolyte	$12 + 3^{b,c}$	18.03 ± 0.20	704 ± 1	72 ± 1	9.15 ± 0.14
MG-207	Mosalyte TDE-250	$8 + 3^{b,c}$	16.12	678	69	7.52
MG-207	Mosalyte TDE-250	$8 + 3^{b,c}$	16.53 ± 0.57	674 ± 4	67 ± 2	7.47 ± 0.04
MG-214	Iodolyte	$14 + 3^a$	16.13	623	70	7.01
MG-214	Iodolyte	$12 + 3^{b,c}$	14.55	660	71	6.83
MG-214	Iodolyte	$12 + 3^{b,c}$	14.68 ± 0.19	657 ± 2	70 ± 1	6.82 ± 0.10
MG-214	Mosalyte TDE-250	$8 + 3^{b,c}$	15.42	609	69	6.52
MG-214	Mosalyte TDE-250	$8 + 3^{b,c}$	15.51 ± 0.49	606 ± 1	67 ± 1	6.32 ± 0.10
RK1	Iodolyte	$10 + 4^a$	18.47 ± 1.39	719 ± 11	70 ± 1	9.28 ± 0.60
RK1	Mosalyte TDE-250	$8 + 3^b$	15.95 ± 0.18	668 ± 1	66 ± 1	7.21 ± 0.14

^a Fabricated and tested at CEA. ^b Fabricated and tested at Solaronix. First line and second line correspond to best cells; third line corresponds to mean-values and standard deviation calculated from at least 3 devices. Dyeing bath: [dye] = 0.2 mM, [CDCA] = 2 mM in MeCN : *t*BuOH 1 : 1, (v/v) except for **MG-207** and **MG-214**. ^c Dyeing bath: [dye] = 0.2 mM, [CDCA] = 2 mM in *CHCl*₃ : EtOH 1 : 1, (v/v).



increase of the charge recombination rate^{42,43} and a conduction band down-shift.³¹

In our dyes, the substitution with phenyl-hexyl groups of the spiro carbon of the indene unit is expected to reduce the dye aggregation. To verify that the aggregation phenomenon is not critical in our solar cells we have fabricated DSSCs without using CDCA. The use of CDCA as co-adsorbent with organic sensitizers is known to diminish the undesirable formation of dye aggregates on the TiO_2 surface.

The results are reported in ESI (Table S5†). We achieved quite comparable performances without CDCA, indicating that aggregation phenomenon is rather limited with these dyes. However, the solar cells show a slightly lower PCE, thus justifying the use of CDCA.

The external quantum efficiency (EQE) was measured for the different solar cells and the spectra are compared in Fig. 4 ($J(V)$ curves are presented in Fig. S19†). The new dyes show a wider photo-response, which is extended towards higher wavelengths compared to **YKP-88**. The results confirm that the dyes embedding a furan spacer are less efficient to convert photons into electrons. This experiment also confirms the good photovoltaic behaviour of the thieno-thiophene based dyes and that **MG-207** is the most efficient dye from this series. IPCE curves and integrated currents of DSSCs are reported in ESI.†

To summarize, with an iodine-containing liquid electrolyte, the new compounds **YKP-137** and **MG-207** exhibit efficiencies quite comparable to **YKP-88**, while the inclusion of a furan spacer in the chemical structure of **DJ-214** and **MG-214** appears to be clearly detrimental to the performances. When tested with an ionic liquid-based electrolyte, all the dyes yield J_{sc} values over 15.4 mA cm^{-2} and two of them *i.e.* **DJ-214** and **MG-207** exhibit a PCE over 7.3%. As previously observed, the devices sensitized by the dyes embedding a furan spacer possess lower V_{oc} (decreased by 30–60 mV). It should be noticed that, with PCEs comprised between 6.52% and 7.52%, our best solar cells rank amongst the most efficient using ionic liquid electrolytes.^{44–46} Besides, these devices are quite robust. For the evaluation of their stability, we subjected them to the standard ISOS-L2 ageing test.⁴⁷ This test consists of continuous irradiation in

a solar simulator with a light intensity of 1000 W m^{-2} at 65°C with ambient relative humidity.⁴⁷ The DSSCs were epoxy-encapsulated and protected with a UV-absorbing polymer (400 nm cut-off). Under these conditions, we found that the solar cells retain more than 85% of their initial performances after 1000 hours. One of the dyes, **YKP-88**, was then subjected to this test for a longer period. Interestingly, the corresponding device demonstrated a high stability and kept 80% of its initial PCE after 6984 hours (291 days). This T_{80} corresponds approximately to 7 years in real conditions (see ESI†).

2.3.2 Co-sensitized dye solar cells. Co-sensitization in DSSCs is a simple and powerful method to increase the PCE.⁴⁸ Using a convenient strategy referred to as “dye cocktails” for the photosensitization, state-of-the-art PCEs of 14.2% and 11.6% with a $[\text{Co}(\text{bpy})_3]^{2+}/^{3+}$ and an I^-/I_3^- redox electrolyte respectively, have been reported in 2020.¹⁵ The co-grafting onto the TiO_2 surface of two properly designed organic dyes affords a compact and robust self-assembled monolayer,¹⁷ which results in a reduction of interfacial charge recombination and an improvement of the V_{oc} . Following this strategy, we combined **YKP-88** and **YKP-137**, two dyes just differing from the alkoxy-chains on the TPA unit, to co-sensitize TiO_2 mesoporous electrodes.

This choice was motivated by their close chemical structure, their good performances and the possibility to benefit from an “umbrella effect” thanks to the alkoxy-groups borne by **YKP-137**. Indeed, bulky substituents on the TPA unit give rise to a physical protection of the TiO_2 surface and prevent the redox electrolyte to recombine with the electrons. The co-sensitized DSSCs were fabricated using dyeing baths containing 0.5 mM of **YKP-88**/**YKP-137** with ratio varying from 8/2 to 2/8 and 5 mM of CDCA. For all compositions, an improvement of the performance was observed with respect to the solar cells sensitized with a single dye (see Table S2 in ESI†). The best performance was achieved for a 6/4 ratio of **YKP-88**/**YKP-137**, for which a J_{sc} of 20.66 mA cm^{-2} , a FF of 71%, a V_{oc} of 745 mV and a PCE of 10.9% was obtained (Fig. 5a).

As expected, the co-sensitization method is an efficient strategy to improve the J_{sc} because the absorption of the photoelectrode is wider with two dyes, but more interestingly, the V_{oc} is also improved.¹⁷ In a DSSC, the V_{oc} is known to correlate with the conduction band edge (E_c) of the semiconductor (TiO_2) and the electron density. The latter is in itself dependent on the rate of recombination between TiO_2 electrons and oxidized electrolyte species. To shed light on the origin of this improvement, charge extraction (CE) and transient photovoltage (TPV) measurements were conducted for the different cells. CE data (Fig. 5b) shows that the co-sensitized device has a higher charge density with respect to the **YKP-88** and the **YKP-137**-based solar cells. This indicates a TiO_2 conduction band shift after co-sensitization compared to other devices. Electron lifetimes measured at identical electron densities are in good agreement with the cell voltages. The electron lifetime (Fig. 5c) for the co-sensitized device is longer than for the solar cells sensitized with a single dye. This suggests a lower propensity for oxide electrons to recombine with redox species in the electrolyte. The benefits of the co-sensitization are also confirmed by the IPCE measurements that clearly show the contribution of

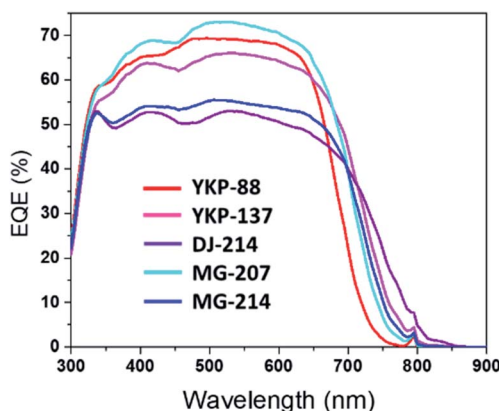


Fig. 4 External Quantum Efficiency (EQE) spectra of solar cells fabricated with **YKP-88**, **YKP-137**, **DJ-214**, **MG-207** and **MG-214**.



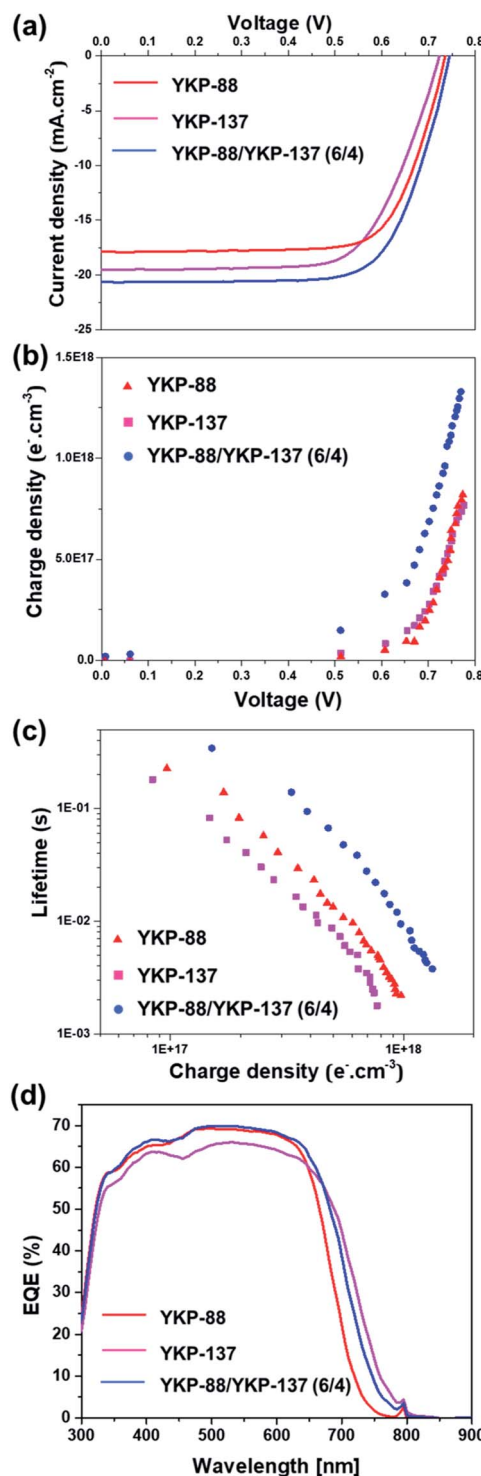


Fig. 5 (a) Current–voltage (J , V) curves for YKP-88, YKP-137 and YKP-88/YKP-137 (6/4) devices, (b) charge extraction data showing electron density as a function of induced voltage for the corresponding DSSCs (c) transient photovoltaic data showing electron lifetimes versus electron density. (d) Comparison of the IPCE spectra of YKP-88-, YKP-137-based solar cells and the co-sensitized device (ratio 6/4).

the two dyes with an increase in the photon-to-electron conversion efficiency and the extension of the photo-response of the cells towards near-infra red region (Fig. 5d).⁵¹

2.3 Fabrication and characterization of mini-modules

One goal of this work was to demonstrate the potential of the new dyes for the fabrication of larger area semi-transparent solar cells. Therefore, we fabricated semi-transparent mini-modules with a 23 cm^2 overall surface area and an active area of 14.08 cm^2 thus representing around 61% of the total area. The mini-modules constitute of five rectangular-shaped cells that are inter-connected in series using a W-type design.⁴⁹ In order to achieve a good photovoltaic performance while keeping an acceptable semi-transparency in the visible, the thickness of the titania electrode was kept at $7\text{--}8\text{ }\mu\text{m}$ without scattering layer.

YKP-88 dye was selected as the photosensitizer because of its good performance and stability in laboratory testing devices and the well-known ruthenium dye **N-719** was employed as a ref. 50.

The manufacturing was done at Solaronix and is fully described in ESI. The **YKP-88** mini-module shows an aesthetic burgundy red tint and possesses an average visible transmittance (AVT) of 26% measured between 380 nm and 740 nm. The first prototype of this 23 cm^2 mini-module showed a current, I_{sc} of 58.1 mA, a V_{oc} of 3.63 V, and a FF of 58.26% leading to a PCE of 8.73% and a power output of 122.9 mW when measured under 1 Sun. This corresponds to a surface power density of 53.4 W m^{-2} (Fig. 6).

These performances are significantly higher than the ones obtained for the reference **N-719** mini-module that exhibited a current, I_{sc} , of 51.8 mA, a V_{oc} of 3.52 V, and a FF of 48.5% leading to a PCE of 6.3% and a power output of 88.5 mW. This

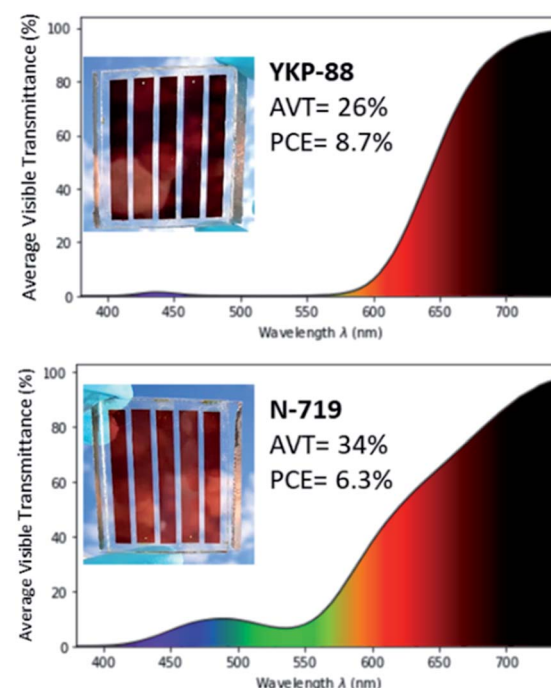


Fig. 6 AVT spectrum of an individual cell from the mini-module, picture and performances for the mini-module fabricated with **YKP-88** (top) and **N-719** (bottom). Figures plotted on python using colour science library.⁵¹



device is more transparent in the blue and green region, and shows an AVT of 34%. This may explain the lower I_{sc} and power conversion performance.

Conclusions

We have designed, synthesised, and characterized four new organic dyes for DSSCs application, and compared their performances with our recently reported reference dye **YKP-88**. The new photosensitizers reveal pink to violet-blue hues and demonstrate PCEs comprised between 7% and 9.8% when used with an iodine-based liquid electrolyte. When an ionic liquid-based electrolyte is employed, the solar cells exhibit PCEs comprised between 6.52% and 7.52%, and retain more than 85% of their initial performance after 1000 hours under ISOS-L2 accelerated ageing conditions. Using one of these molecules *i.e.* **YKP-137** in combination with **YKP-88** in a co-sensitization approach, the PCEs of the solar cells are improved up to 10.9% and we demonstrate that better photo-injection of electrons and lower recombination rates are responsible for the simultaneous increase of the J_{sc} and V_{oc} .

Finally, we demonstrate that **YKP-88** can be successfully incorporated in solar mini-modules with an active area of 14 cm² (total area 23 cm²), exhibiting a transparency in the visible of 26% and a power output of *circa* 123 mW corresponding to a surface power of 53.4 W m⁻². This work highlights the potential of this new generation of organic dyes for future applications in semi-transparent solar cells.

Author's contribution

M. G., D. J. and Y. K. performed the synthesis and characterization of the dyes. M. G., S. N., V. M. M. and F. O. fabricated and characterized the solar cells and mini-modules. J. L. performed the DFT calculation and characterized the mini-modules optically. C. A., L. C., and E. P. performed the photo-physical characterization of the solar cells. C. A. G. F. and G. O. carried out a preliminary study on device optimization. Q. H. analysed the data and prepared the first draft of the manuscript. R. D. designed the materials and experiments, supervised the work, analysed the data and wrote the manuscript with contributions of all the co-authors.

Conflicts of interest

R. D. and Y. K. are employees of CEA, which holds a patent on this technology (Inventors: R. D., D. J., M. G. and Y. K.; current assignee: Commissariat à l'Energie Atomique et aux Energies Alternatives; number: WO2017194368A1; date of publication: 16/11/2017). S. N is currently an employee of Solaronix that holds a license on this technology and that sells electrodes and chemical components that were used in this study.

Acknowledgements

R. D. acknowledges ANR for funding through the ODYCE project (grant agreement number ANR-14-OHRI-0003-01). J. L.

acknowledges CEA for funding through a CFR PhD grant. R. D. acknowledges the European Research Council (ERC) for funding. This work was partially funded under the European Union's Horizon 2020 research and innovation programme (grant agreement number 832606; project PISCO). E. P. acknowledges the ICIQ and ICREA for financial support. R. D. acknowledges the LABEX Laboratoire d'Alliances Nanosciences-Energies du Futur (LANEF, ANR-10-LABX-51-44001) for funding and the Hybriden Facility at CEA-Grenoble. C. A. acknowledges the UGA and EDCSV for funding. G. O. acknowledges funding from Conacyt under grant number CB_2017-2018_A1-S-21018. R. D. thanks Jacques Pécaut for solving the X-Ray crystal structures presented in ESI and José Sanchez for his help in measuring the IPCE spectra.

Notes and references

- 1 B. Hallam, *et al.*, Eliminating Light-Induced Degradation in Commercial p-Type Czochralski Silicon Solar Cells, *Applied Science*, 2018, **8**, 10.
- 2 S. Pizzini, Towards solar grade silicon: Challenges and benefits for low cost photovoltaics, *Sol. Energy Mater. Sol. Cells*, 2010, **94**, 1528–1533.
- 3 C.-T. Li, Y.-L. Kuo, C. P. Kumar, P.-T. Huang and J. T. Lin, Tetraphenylethylene tethered phenothiazine-based double-anchored sensitizers for high performance dye-sensitized solar cells, *J. Mater. Chem. A*, 2019, **7**, 23225–23233.
- 4 Y. Ren, *et al.*, A Blue Photosensitizer Realizing Efficient and Stable Green Solar Cells via Color Tuning by the Electrolyte, *Adv. Mater.*, 2020, **32**, 2000193.
- 5 P. Cheng, G. Li, X. Zhan and Y. Yang, Next-generation organic photovoltaics based on non-fullerene acceptors, *Nat. Photonics*, 2018, **12**, 131–142.
- 6 L. Meng, *et al.*, Organic and solution-processed tandem solar cells with 17.3% efficiency, *Science*, 2018, **361**, 1094–1098.
- 7 S. A. Hashemi, S. Ramakrishna and A. G. Aberle, Recent progress in flexible-wearable solar cells for self-powered electronic devices, *Energy Environ. Sci.*, 2020, **13**, 685–743.
- 8 A. Cannavale, *et al.*, Perovskite photovoltachromic cells for building integration, *Energy Environ. Sci.*, 2015, **8**, 1578–1584.
- 9 X. Lin, *et al.*, Efficiency progress of inverted perovskite solar cells, *Energy Environ. Sci.*, 2020, DOI: 10.1039/D0EE02017F.
- 10 M. A. Green, K. Emery, Y. Hishikawa, W. Warta and E. D. Dunlop, Solar cell efficiency tables (version 47), *Prog. Photovoltaics*, 2016, **24**, 3–11.
- 11 K. Kakiage, *et al.*, Highly-efficient dye-sensitized solar cells with collaborative sensitization by silyl-anchor and carboxy-anchor dyes, *Chem. Commun.*, 2015, **51**, 15894–15897.
- 12 S. Mathew, *et al.*, Dye-sensitized solar cells with 13% efficiency achieved through the molecular engineering of porphyrin sensitizers, *Nat. Chem.*, 2014, **6**, 242–247.
- 13 Z. Yao, *et al.*, Dithienopicenocarbazole as the kernel module of low-energy-gap organic dyes for efficient conversion of sunlight to electricity, *Energy Environ. Sci.*, 2015, **8**, 3192–3197.



14 Y. Ren, *et al.*, A Stable Blue Photosensitizer for Color Palette of Dye-Sensitized Solar Cells Reaching 12.6% Efficiency, *J. Am. Chem. Soc.*, 2018, **140**, 2405–2408.

15 J.-M. Ji, H. Zhou, Y. K. Eom, C. H. Kim and H. K. Kim, 14.2% Efficiency Dye-Sensitized Solar Cells by Co-sensitizing Novel Thieno[3,2-b]indole-Based Organic Dyes with a Promising Porphyrin Sensitizer, *Adv. Energy Mater.*, 2020, **10**, 2000124.

16 D. Joly, *et al.*, A Robust Organic Dye for Dye Sensitized Solar Cells Based on Iodine/Iodide Electrolytes Combining High Efficiency and Outstanding Stability, *Sci. Rep.*, 2014, **4**, 4033.

17 P. Wang, *et al.*, Stable and Efficient Organic Dye-Sensitized Solar Cell Based on Ionic Liquid Electrolyte, *Joule*, 2018, **2**, 2145–2153.

18 A. Fakharuddin, R. Jose, T. M. Brown, F. Fabregat-Santiago and J. Bisquert, A perspective on the production of dye-sensitized solar modules, *Energy Environ. Sci.*, 2014, **7**, 3952–3981.

19 H. Yuan, *et al.*, Outdoor testing and ageing of dye-sensitized solar cells for building integrated photovoltaics, *Sol. Energy*, 2018, **165**, 233–239.

20 S. Yoon, S. Tak, J. Kim, Y. Jun, K. Kang and J. Park, Application of transparent dye-sensitized solar cells to building integrated photovoltaic systems, *Building and Environment*, 2011, **46**, 1899–1904.

21 D. Joly, *et al.*, Metal-free organic sensitizers with narrow absorption in the visible for solar cells exceeding 10% efficiency, *Energy Environ. Sci.*, 2015, **8**, 2010–2018.

22 M. K. Nazeeruddin, A. Kay, I. Rodicio, R. Humphry-Baker, E. Mueller, P. Liska, N. Vlachopoulos and M. Graetzel, Conversion of light to electricity by *cis*-X2bis(2,2'-bipyridyl-4,4'-dicarboxylate)ruthenium(II) charge-transfer sensitizers (X = Cl⁻, Br⁻, I⁻, CN⁻, and SCN⁻) on nanocrystalline titanium dioxide electrodes, *J. Am. Chem. Soc.*, 1993, **115**, 6382–6390.

23 S. Aghazada and M. K. Nazeeruddin, Ruthenium Complexes as Sensitizers in Dye-Sensitized Solar Cells, *Inorganics*, 2018, **6**, 52.

24 A. Mishra, M. K. R. Fischer and P. Bäuerle, Metal-Free Organic Dyes for Dye-Sensitized Solar Cells: From Structure: Property Relationships to Design Rules, *Angew. Chem., Int. Ed.*, 2009, **48**, 2474–2499.

25 C.-P. Lee, *et al.*, Recent progress in organic sensitizers for dye-sensitized solar cells, *RSC Adv.*, 2015, **5**, 23810–23825.

26 S. P. Singh and T. Gayathri, Evolution of BODIPY Dyes as Potential Sensitizers for Dye-Sensitized Solar Cells, *Eur. J. Org. Chem.*, 2014, 4689–4707.

27 C. Aumaitre, *et al.*, Visible and near-infrared organic photosensitizers comprising isoindigo derivatives as chromophores: synthesis, optoelectronic properties and factors limiting their efficiency in dye solar cells, *J. Mater. Chem. A*, 2018, **6**, 10074–10084.

28 H.-L. Jia, *et al.*, Efficient cosensitization of new organic dyes containing bipyridine anchors with porphyrins for dye-sensitized solar cells, *Sustainable Energy Fuels*, 2019, **4**, 347–353.

29 J. Yang, *et al.*, Efficient and stable organic DSSC sensitizers bearing quinacridone and furan moieties as a planar π-spacer, *J. Mater. Chem.*, 2012, **22**, 24356–24365.

30 L. Xu, *et al.*, Increasing the Efficiency of Organic Dye-Sensitized Solar Cells over 10.3% Using Locally Ordered Inverse Opal Nanostructures in the Photoelectrode, *Adv. Funct. Mater.*, 2018, **28**, 1706291.

31 S. Qu, *et al.*, New diketo-pyrrolo-pyrrole (DPP) sensitizer containing a furan moiety for efficient and stable dye-sensitized solar cells, *Dyes Pigm.*, 2012, **92**, 1384–1393.

32 A. Covezzi, *et al.*, 4D-π-1A type β-substituted ZnII-porphyrins: ideal green sensitizers for building-integrated photovoltaics, *Chem. Commun.*, 2016, **52**, 12642–12645.

33 R. Venkatraman, S. V. K. Panneer, E. Varathan and V. Subramanian, Aromaticity-Photovoltaic Property Relationship of Triphenylamine-Based D-π-A Dyes: Leads from DFT Calculations, *J. Phys. Chem. A*, 2020, **124**, 3374–3385.

34 W. Sharmoukh, J. Cong, B. A. Ali, N. K. Allam and L. Kloof, Comparison between Benzothiadiazole-Thiophene- and Benzothiadiazole-Furan-Based D-A-π-A Dyes Applied in Dye-Sensitized Solar Cells: Experimental and Theoretical Insights, *ACS Omega*, 2020, **5**, 16856–16864.

35 W. Zhang, *et al.*, Rational Molecular Engineering of Indoline-Based D-A-π-A Organic Sensitizers for Long-Wavelength-Responsive Dye-Sensitized Solar Cells, *ACS Appl. Mater. Interfaces*, 2015, **7**, 26802–26810.

36 G. A. Sewvandi, *et al.*, Interplay between Dye Coverage and Photovoltaic Performances of Dye-Sensitized Solar Cells Based on Organic Dyes, *J. Phys. Chem. C*, 2014, **118**, 20184–20192.

37 T. A. Oudenhoven, Y. Joo, J. E. Laaser, P. Gopalan and M. T. Zanni, Dye aggregation identified by vibrational coupling using 2D IR spectroscopy, *J. Chem. Phys.*, 2015, **142**, 212449.

38 A. F. Buene, N. Boholm, A. Hagfeldt and B. H. Hoff, Effect of furan π-spacer and triethylene oxide methyl ether substituents on performance of phenothiazine sensitizers in dye-sensitized solar cells, *New J. Chem.*, 2019, **43**, 9403–9410.

39 H. Song, X. Li, H. Ågren and Y. Xie, Branched and linear alkoxy chains-wrapped push-pull porphyrins for developing efficient dye-sensitized solar cells, *Dyes Pigm.*, 2017, **137**, 421–429.

40 F. Lu, *et al.*, Novel D-π-A porphyrin dyes with different alkoxy chains for use in dye-sensitized solar cells, *Dyes Pigm.*, 2016, **125**, 116–123.

41 A. Yella, *et al.*, Molecular Engineering of a Fluorene Donor for Dye-Sensitized Solar Cells, *Chem. Mater.*, 2013, **25**, 2733–2739.

42 H. Jia, X. Ju, M. Zhang, Z. Ju and H. Zheng, Effects of heterocycles containing different atoms as π-bridges on the performance of dye-sensitized solar cells, *Phys. Chem. Chem. Phys.*, 2015, **17**, 16334–16340.

43 L. Cabau, *et al.*, A single atom change “switches-on” the solar-to-energy conversion efficiency of Zn-porphyrin based



dye sensitized solar cells to 10.5%, *Energy Environ. Sci.*, 2015, **8**, 1368–1375.

44 M. Gorlov and L. Kloo, Ionic liquid electrolytes for dye-sensitized solar cells, *Dalton Trans.*, 2008, 2655–2666, DOI: 10.1039/B716419J.

45 Y. Fang, *et al.*, Synthesis of Low-Viscosity Ionic Liquids for Application in Dye-Sensitized Solar Cells, *Chem.-Asian J.*, 2019, **14**, 4201–4206.

46 W. Zeng, *et al.*, Efficient Dye-Sensitized Solar Cells with an Organic Photosensitizer Featuring Orderly Conjugated Ethylenedioxothiophene and Dithienosilole Blocks, *Chem. Mater.*, 2010, **22**, 1915–1925.

47 M. V. Khenkin, *et al.*, Consensus statement for stability assessment and reporting for perovskite photovoltaics based on ISOS procedures, *Nat. Energy*, 2020, **5**, 35–49.

48 J. M. Cole, G. Pepe, O. K. Al Bahri and C. B. Cooper, Cossensitization in Dye-Sensitized Solar Cells, *Chem. Rev.*, 2019, **119**, 7279–7327.

49 F. Giordano, E. Petrolati, T. M. Brown, A. Reale and A. Di Carlo, Series-Connection Designs for Dye Solar Cell Modules, *IEEE Trans. Electron Devices*, 2011, **58**, 2759–2764.

50 M. Grätzel, Solar Energy Conversion by Dye-Sensitized Photovoltaic Cells, *Inorg. Chem.*, 2005, **44**, 6841–6851.

51 T. Mansencal, *et al.*, Colour 0.3.15, 2020, DOI: 10.5281/zenodo.3627408.

